RSC Advances

ROYAL SOCIETY OF CHEMISTRY

PAPER

View Article Online
View Journal | View Issue

Check for updates

Cite this: *RSC Adv.*, 2025, **15**, 17685

Half-metallicity of novel halide double perovskites K_2CuVCl_6 and Rb_2CuVCl_6: application in next-generation spintronic devices

Mohammed El Amine Monir,[a] Hadj Baltach,[a] K. Bouferrache,[bc] M. Fatmi,[b] M. A. Ghebouli,[bd] Faisal Katib Alanazi,*[e] B. Ghebouli,[f] Maroua Imène Benamrani[g] and Rabah Boudissa[bf]

Received 22nd April 2025
Accepted 12th May 2025

DOI: 10.1039/d5ra02811f

rsc.li/rsc-advances

This work reports the determination of structural, electronic, half-metallic and magnetic properties of new double perovskites K_2CuVCl_6 and Rb_2CuVCl_6 using the full-potential linearized augmented plane wave plus local orbitals method incorporated in the WIEN2k code. The calculations performed for this prediction were framed using the density functional theory, and the exchange and correlation potential were described using the generalized gradient approximation of TB-mBJ (Tran–Blaha modified Becke–Johnson). The structural properties confirmed the stable ferromagnetic ground state of the two studied compounds. The equilibrium structural parameters, such as lattice constant (a_0), bulk modulus (B_0), their first pressure derivative (B') and minimum of the total energy (E_0), were determined for both the compounds. The electronic properties showed that the studied perovskite compounds were completely half-metallic materials. The half-metallic gap (E_{HM}) values for the compounds were 1.119 eV (for K_2CuVCl_6) and 1.088 eV (for Rb_2CuVCl_6). The exchange-splitting energy ($\Delta(d)$) was found to be large for both the compounds ($\Delta(d) = 3.482$ eV for K_2CuVCl_6 and $\Delta(d) = 3.380$ eV for Rb_2CuVCl_6). The calculated total magnetic moments of the two studied materials indicated major contributions from V atoms and minor contributions from Cu atoms. Owing to p–d hybridization, feeble magnetic moments were exhibited by the non-magnetic K, Rb, Cu and Cl sites, while the atomic magnetic moment of V atoms decreased from its free space charge of 3.00 μ_B.

1. Introduction

Half-metallic materials play vital roles in the development of new devices based on spintronic and optoelectronic technologies. In the last decade, half-metallic materials have attracted increasing attention of researchers owing to their excellent electronic, magnetic and optical properties. Generally, half-metallic compounds exhibit two different electronic behaviors depending on the two spin directions: a semiconducting character in one spin direction and a metallic nature in the other spin direction.[1] Research in this domain was initiated by the prediction of the electronic structure of half-Heuslers NiMnS and PtMnS by Groot *et al.*[2] The most prominent works after this prediction were on perovskite materials, such as $La_{0.70}Sr_{0.30}MnO_3$ and Sr_2FeMoO_6;[3,4] Heusler alloys, such as Co_2MnSi and Co_2FeSi;[5,6] and TM-doped chalcogenide and pnictide semiconductors.[7]

In the present time, the half-metallicity has appeared in several types of materials, such as: TM (transition metal) doped semiconductors, exploring half-metallicity in NiO *via* TM and NTM doping: Insights from LDA and LDA-SIC approaches,[8] investigating half-metallic behavior of MnO doped with TM and NTM: LDA, LDA-SIC and LDA + *U* analysis;[9] half-Heusler alloys, study on the phase stability, mechanical and half-metallic properties of half-Heusler alloys FeMnZ (Z = Si, Ge and Sn),[10] half-metallicity and thermoelectric performance: A multifaceted investigation of Zr-based half-Heusler alloys;[11] full-Heusler alloys, a spin-polarized analysis of the half-metallicity, mechanical, structural and optoelectronic attributes of full-Heusler $XVCo_2$ (X = B and P) alloys,[12] revealing half-metallicity: predicting large band-gaps in halogen-based full-Heusler alloys;[13] quaternary Heusler alloys, systematic study of

---

[a] Faculty of the Exact Sciences, Mustapha Stambouli University of Mascara, B. P. 305, 29000 Mascara, Algeria

[b] Research Unit on Emerging Materials (RUEM), University Ferhat Abbas of Setif 1, Setif, 19000, Algeria

[c] Department of Physics, Faculty of Sciences, University of M'sila University Pole, Road Bourdj Bou Arreiridj, 28000, M'sila, Algeria

[d] Department of Chemistry, Faculty of Sciences, University of M'sila University Pole, Road Bourdj Bou Arreiridj, 28000, M'sila, Algeria

[e] Department of Physics, College of Sciences, Northern Border University, P. O. Box 1321, 91431 Arar, Saudi Arabia. E-mail: faisal.katib.al@gmail.com

[f] Laboratory for the Study of Surfaces and Interfaces of Solid Materials (LESIMS), University Ferhat Abbas of Setif 1, Setif, 19000, Algeria

[g] Laboratoire de Croissance et Caractérisation de Nouveaux Semiconducteurs (LCCNS), Faculté de Technologie, Université Ferhat Abbas Setif 1, 19000 Setif, Algeria

structural, elastic, electronic, magnetism and half-metallic properties for the quaternary alloys: Heusler type VZrReZ (Z = Si, Ge and Sn),[14] *ab initio* study of quaternary Heusler alloys LiAEFeSb (AE = Be, Mg, Ca, Sr or Ba) and prediction of half-metallicity in LiSrFeSb and LiBaFeSb;[15] perovskites materials, a DFT theoretical prediction of new half-metallic ferromagnetism, mechanical stability, optoelectronic and thermoelectric properties of $ZnCrO_3$ perovskites for spintronic applications,[16] half-metallic ferromagnetic and optical properties of $YScO_3$ (Y = Ni, Pd, and Pt) perovskite: a first principles study;[17] and double perovskite materials, harnessing the half-metallicity and thermoelectric insights in Cs_2AgMBr_6 (M = V, Mn, Ni) double halide perovskites: a DFT study,[18] tunability of half metallicity and thermoelectric indicators in Na_2TaX_6 (X = Cl, Br) vacancy ordered double perovskites.[19] Moreover, recent studies have highlighted the growing interest in simple and double perovskites owing to their tunable properties and potential in optoelectronics, catalysis, and energy applications.[20–33]

In this study, we computed the structural, electronic and magnetic features of the new double perovskites K_2CuVCl_6 and Rb_2CuVCl_6 in order to prove their complete half-metallic property, and the calculations were carried out using the full-potential linearized augmented plane waves with local orbitals (FP-LAPW + lo) method embedded in the WIEN2k package. This study was conducted in order to determine the large half-metallic energy gap (E_{HM}) and high Curie temperature (T_C) corresponding to the new double perovskites K_2CuVCl_6 and Rb_2CuVCl_6 using the TB-mBJ–GGA approximation. This study is crucial for the development of spintronics, enabling low-energy storage and computing devices. It also highlights the prospects of these materials in optoelectronics, particularly for advanced LEDs and solar cells. Finally, these findings can be utilized in thermoelectricity to enhance the energy efficiency of industrial systems.

The rest of this article is given as follows: simulation method and calculation details are mentioned in Section 2. Obtained results are discussed in Section 3. The conclusions of this prediction are listed in Section 4.

2. Computational details

In this work, the DFT (density functional theory)[34] calculations were carried out by employing the full-potential linearized augmented plane waves plus local orbitals (FP-LAPW + lo) method[35,36] implemented in the WIEN2k code.[37] The potential of exchange and correlation is described using both Perdew–Burke–Ernzerhof generalized gradient approximation (PBE–GGA)[38] and Tran–Blaha modified Becke–Johnson potential of the generalized gradient approximation (TB-mBJ–GGA).[39,40] The computational parameters employed in this prediction approach are as follows: the matrix size $R_{MT} \times K_{max}$ parameter, which represents the extension of the plane waves and the convergence of the energy eigenvalues, is taken as 8, where K_{max} denotes the large modulus of the reciprocal lattice vector, and R_{MT} denotes the small radius of muffin-tin spheres. The cut-off energy ($E_{cut\text{-}off}$), which evaluates the number of plane waves used in the basic function, was chosen as −6 eV. The Fourier expansion factor (G_{Max}) that describes charge density translation and wave function expansion was set to 12. The irreducible Brillouin zone integrations were founded on the 11 × 11 × 11 mesh, in which 56 *k*-points were produced. The maximum norm of the angular momentum was equal to $l_{max} = 10$. The computed radii of the K, Rb, Cu, V, and Cl atoms reported in this study were 2.50, 2.50, 2.35, 2.30 and 2.02 a.u., respectively. The K ($4s^1$), Rb ($5s^1$), Cu ($3d^{10}4s^1$), V ($3d^3 4s^2$) and Cl ($3s^2 3p^5$) states were treated as valence electrons. The antiferromagnetic calculations were carried out using the supercell size of 1 × 1 × 2. Furthermore, the self-consistent process was set to stop iterations when the convergence energy becomes greater than 10^{-4} Ry.

3. Results and discussion

3.1. Structural properties

3.1.1. Crystal structure. The current double perovskites X_2CuVCl_6 (X = K and Rb) crystallize in the cubic system with the space group $Fm\bar{3}m$ (no. 225).[41] The atomic positions are given as follows: the X atoms occupy the 8c (1/4, 1/4, 1/4) positions, the Cu and V atoms occupy the 4a (0, 0, 0) and 4b (1/2, 0, 0) positions, respectively, and Cl atoms are located at the 24e (0.2504, 0, 0) positions.[41] The crystal structure of the double perovskite compound is depicted in Fig. 1.

3.1.2. The equilibrium lattice parameters of the studied double perovskites. The optimized structural parameters were fitted using the empirical Birch–Murnaghan equation of state (EOS).[42,43] The fitted *E*–*V* curves of the K_2CuVCl_6 and Rb_2CuVCl_6

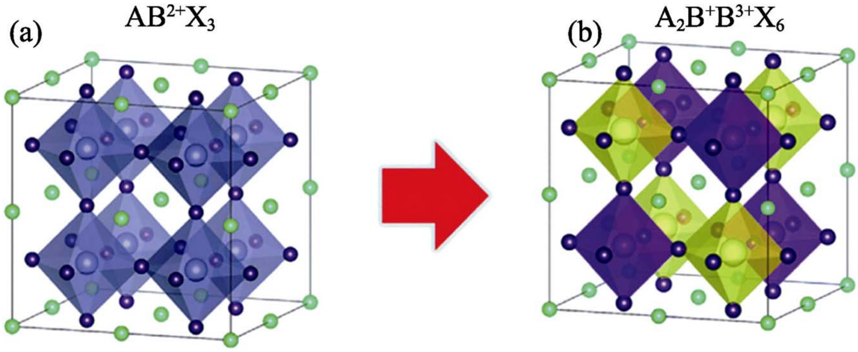

Fig. 1 Crystal structure of (a) ABX_3 simple perovskite and (b) $A_2BB'X_6$ double perovskite compounds (A = K and Rb, B = Cu, B′ = V and X = Cl).

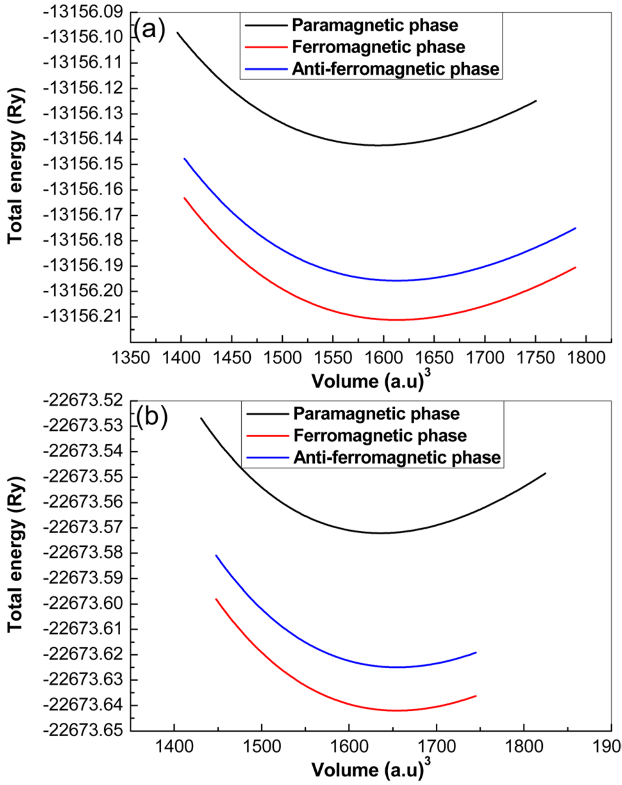

Fig. 2 Plot of total energy fitting *versus* cell-volume of (a) K_6CuVCl_6 and (b) Rb_6CuVCl_6 double perovskite compounds.

double perovskites obtained using the framework of the Birch–Murnaghan equation in the paramagnetic (PM), ferromagnetic (FM) and anti-ferromagnetic (AFM) phases are illustrated in Fig. 2. It can be observed that the ferromagnetic state is the stable ground phase for all the studied compounds. The optimized structural parameters, such as the equilibrium lattice constant (a_0), bulk modulus (B_0), its first pressure derivative (B') and the minimum of the total energy (E_0), of both K_2CuVCl_6 and Rb_2CuVCl_6 are summarized in Table 1. No experimental data or theoretical values have been reported in the literature for these double perovskite materials, so our structural results of these K_2CuVCl_6 and Rb_2CuVCl_6 compounds are more and more useful for further experimental and predicted works in the spintronic and optoelectronic areas.

3.1.3. Cohesive energy and formation energy

3.1.3.1. Cohesive energy. In a solid, the atoms are bound together by cohesive energy (E_{Coh}). The E_{Coh} energy value is estimated as the difference between the total energy of the material and the sum of different atomic energies of the constituents at infinite separation.[45] The E_{Coh} energy of the X_2CuVCl_6 (X = K and Rb) materials was calculated using the following formula:

$$E_{Coh}(X_2CuVCl_6) = (2E^X + E^{Cu} + E^V + 6E^{Cl}) - E_0 \quad (1)$$

where E^X, E^{Cu}, $E^V$and E^{Cl} represent the constituent energies of X, Cu, V and Cl atoms, respectively; and E_0 indicates the total energy of the solid. The calculated E_{Coh} energies of the current compounds at their ferromagnetic stable state are listed in Table 2. The E_{Coh} energies of both compounds have a positive sign, which confirms that the compounds are stable in the ferromagnetic phase.

3.1.3.2. Formation energy. Formation energy (E_f) is the energy required for maintaining material stability in its favorable crystalline structure under the theoretical temperature of 0 K; the negative value of E_f denotes the stable structure of the material and confirms the strong bonding between the atoms in their favorable crystal structure.[46]

The E_f energy of the studied X_2CuVCl_6 (X = K and Rb) compounds was calculated according to the following relationship:

$$E_f(X_2CuVCl_6) = E_0 - (2E^X + E^{Cu} + E^V + 6E^{Cl}) \quad (2)$$

Table 1 Equilibrium lattice parameters of X_6CuVCl_6 (X = K and Rb) double perovskite materials in PM, FM and AFM phases calculated using the GGA approximation. The results are compared with those of the $K_2ScCuCl_6$ and $Rb_2ScCuCl_6$ double perovskite compounds

Material	Configuration	Lattice constant a_0 (Å)	Bulk modulus B_0 (GPa)	B'	Minimum of the total energy E_0 (Ry)
K_2CuVCl_6	PM phase	9.8142	40.7357	4.8572	−13156.1424
	FM phase	9.8513	39.0165	5.1508	−13156.2112
	AFM phase	9.8417	39.0712	4.9912	−13156.1957
Rb_2CuVCl_6	PM phase	9.8978	39.6915	4.9354	−22673.5721
	FM phase	9.9357	38.3989	4.9421	−22673.6420
	AFM phase	9.9214	38.4157	4.9321	−22673.6249
$K_2ScCuCl_6$ (ref. 44)	PM phase	9.98	35.76	5.00	−12786.28
$Rb_2ScCuCl_6$ (ref. 44)	PM phas	10.08	49.09	8.47	−22303.72

Table 2 Computed cohesive energy E_{Coh} (in Ry) of the equilibrium X_6CuVCl_6 (X = K and Rb) double perovskite materials and energies of individual X, Cu, V and Cl atoms

Material	E_0	E^X	E^{Cu}	E^V	E^{Cl}	E_{Coh}
K_2CuVCl_6	−13156.211232	−1204.191254	−3309.685742	−1898.056927	−922.888706	2.753819
Rb_2CuVCl_6	−22673.642044	−5962.915605	−3309.685748	−1898.056928	−922.888707	2.735916

Table 3 Computed formation energy E_f (in Ry) of the equilibrium X_6CuVCl_6 (X = K and Rb) double perovskite materials and atomic energies of the X, Cu, V and Cl atoms in their stable ferromagnetic ground phase. The results are compared with those of the $K_2ScCuCl_6$ and $Rb_2ScCuCl_6$ double perovskite compounds

Material	E_0	E^X	E^{Cu}	E^V	E^{Cl}	E_f
K_2CuVCl_6	−13156.211232	−1204.200105	−3309.691002	−1898.059868	−922.890102	−2.719540
Rb_2CuVCl_6	−22673.642044	−5962.920203	−3309.691002	−1898.059868	−922.890102	−2.710156
$K_2ScCuCl_6$ (ref. 44)	−12786.28	—	—	—	—	−2.75
$Rb_2ScCuCl_6$ (ref. 44)	−22303.72	—	—	—	—	−2.27

where E^X, E^{Cu}, E^V and E^{Cl} are the corresponding atomic energies in their crystal structure, while E_0 is the total energy of the material; the obtained values of E_F energy are tabulated in Table 3. The negative E_F energy values obtained for all compounds (Table 3) strongly confirm that these materials are stable in their perovskite crystal structure.

3.1.4. Dynamic stability. The computed phonon dispersion curves of the studied X_2CuVCl_6 (X = K and Rb) materials are depicted in Fig. 3 along the R–Γ–X–Z–M–Γ path in the three-dimensional (3D) Brillouin zone. It can be seen that the imaginary frequency modes (frequencies with a negative sign) are absent in the phonon dispersion curves of both compounds, which confirms their dynamic stability.

3.2. Elastic properties

The elasticity tensor of a cubic system is defined by three independent elastic constants, namely C_{11}, C_{12} and C_{44}. The elastic constants (C_{11}, C_{12} and C_{44}) of the X_2CuVCl_6 (X = K and Rb) materials were computed using the IRelast program[47] implemented in the WIEN2k package,[23] and the values obtained by the GGA approximation are shown in Table 4. The Born's criteria[48,49] for assessing the mechanical stability of materials that crystallize in the cubic system are as follows:[48,49]

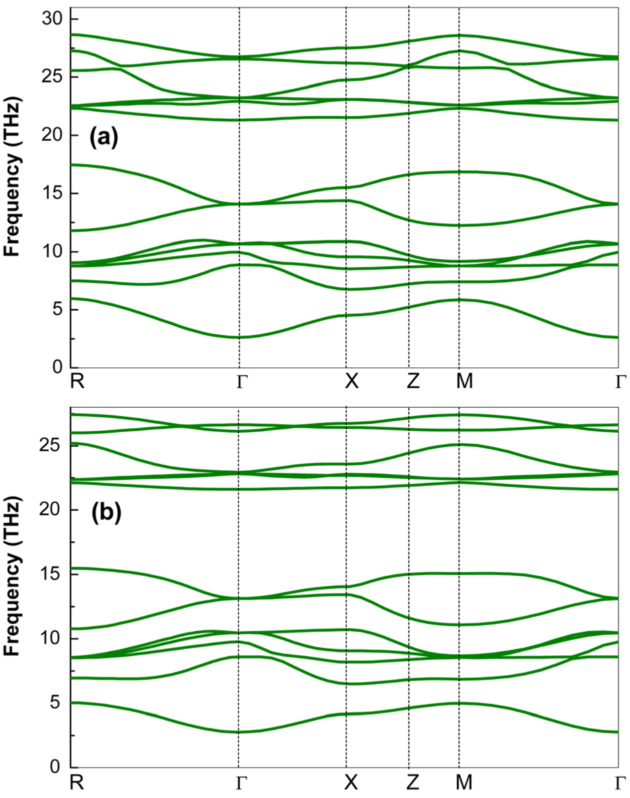

Fig. 3 Phonon dispersion of (a) K_2CuVCl_6 and (b) Rb_2CuVCl_6 double perovskite materials along the R–Γ–X–Z–M–Γ path.

$$\begin{cases} (C_{11} - C_{12}) > 0 \\ (C_{11} + 2C_{12}) > 0 \\ C_{11} > 0 \\ C_{44} > 0 \\ C_{12} < B < C_{11} \end{cases} \tag{3}$$

Therefore, the GGA results confirm that the studied X_2CuVCl_6 (X = K and Rb) compounds are mechanically stable.

The shear modulus (G) is defined as a parameter for evaluating the resistance of a material to plastic strain; it is calculated as the average of the Voigt[50] and Reuss[51] approaches, and it is reformulated according to the Hill's approach:[52]

$$G = \frac{G_V + G_R}{2} \tag{4}$$

where

$$\begin{cases} G_V = \dfrac{C_{11} - C_{12} + 3C_{44}}{5} \\ G_R = \dfrac{5C_{44}(C_{11} - C_{12})}{4C_{44} + 3(C_{11} - C_{12})} \end{cases} \tag{5}$$

Bulk modulus (B_0) is the factor that determines the resistance to fracture.[53] Moreover, Pugh's ratio (B_0/G) is another parameter that identifies the brittleness and ductility of

Table 4 Elastic constants C_{ij} (in GPa), bulk modulus B_0 (in GPa), shear modulus G and Pugh's ratio B_0/G of the equilibrium X_6CuVCl_6 (X = K and Rb) double perovskite materials in their stable ferromagnetic ground state calculated using the GGA approximation. The results are compared with those of the $K_2ScCuCl_6$ and $Rb_2ScCuCl_6$ double perovskite compounds

Material	C_{11}	C_{12}	C_{44}	B_0	G	B_0/G
K_2CuVCl_6	69.512	23.012	7.561	38.512	12.096	3.184
Rb_2CuVCl_6	91.473	11.110	11.242	37.898	19.304	1.963
$K_2ScCuCl_6$ (ref. 44)	68.63	16.76	6.83	34.15	11.75	2.91
$Rb_2ScCuCl_6$ (ref. 44)	89.74	28.43	10.27	48.87	16.01	3.05

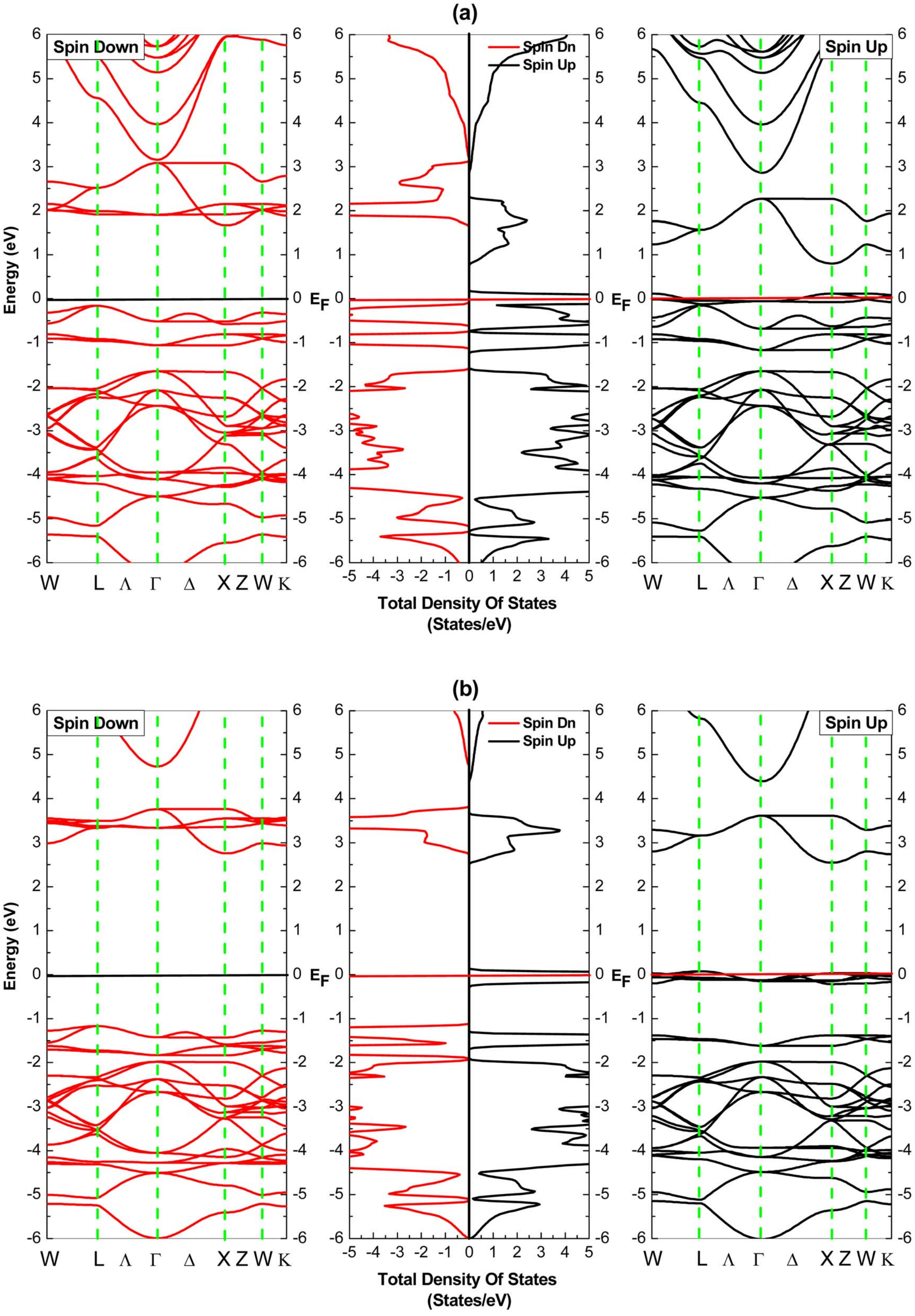

Fig. 4 Spin-polarized electronic structure of the equilibrium double perovskite K_2CuVCl_6 calculated using (a) PBE–GGA and (b) TB-mBJ–GGA functionals.

materials.[54,55] The material becomes brittle when the B_0/G parameter is less than 1.75; when the value is higher ($B_0/G > 1.75$), the material will have a ductile nature. According to the Pugh ratios reported in Table 4, the present materials are ductile materials. Therefore, the two studied materials are held in their form by metallic bonding.

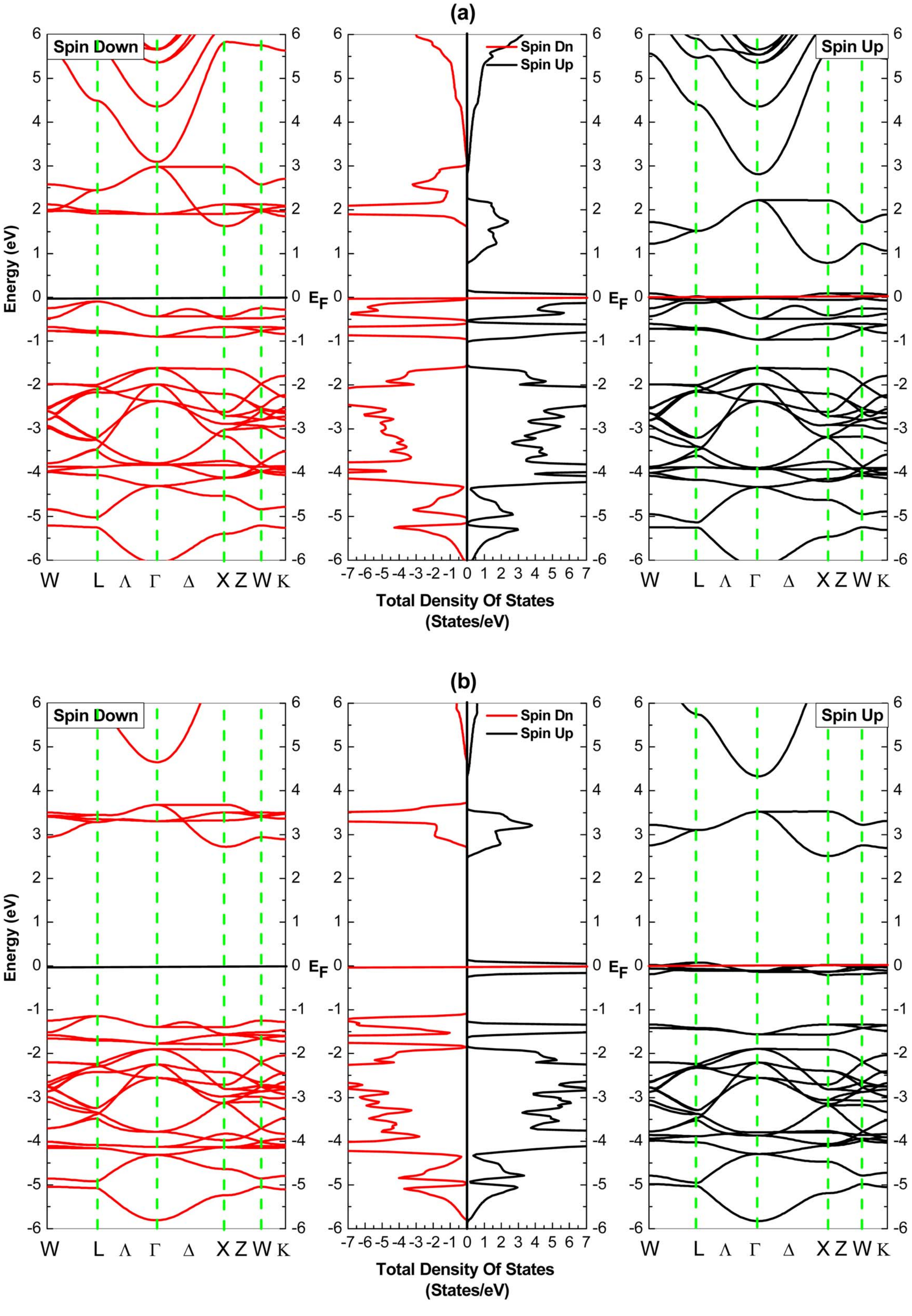

Fig. 5 Spin-polarized electronic structure of the equilibrium double perovskite Rb_2CuVCl_6 calculated using (a) PBE–GGA and (b) TB-mBJ–GGA functionals.

3.3. Electronic properties

In this work, the electronic band structures and density of states of the double perovskite materials K_2CuVCl_6 and Rb_2CuVCl_6 were predicted using both GGA and TB-mBJ–GGA functionals, aiming to explore their electronic properties and assess their potential for practical applications.

3.3.1. Spin-polarized electronic band structures. The spin-polarized electronic band structures of the equilibrium K_2CuVCl_6 and Rb_2CuVCl_6 compounds were evaluated along the high-symmetry directions and are presented in Fig. 4 and 5, respectively. The differences observed between the GGA and TB-mBJ–GGA results highlight a pronounced exchange splitting between the spin-up and spin-down channels. Specifically, the spin-up band structures of both compounds exhibit metallic behavior, as evidenced by the overlap between the valence and conduction bands. In contrast, the spin-down band structures display semiconducting characteristics, with the Fermi level positioned within a distinct energy gap. Therefore, the studied double perovskite materials strongly exhibit a complete half-metallic nature in the cubic structure. Moreover, the half-metallic gap (E_{HM}) of each equilibrium material was evaluated in order to determine the Curie temperature. First, the E_{HM} gap energy is defined as the minimum between the lowest energies of the minority-spin and majority-spin conduction bands with respect to the Fermi level, and the absolute values of the highest energies of minority-spin and majority-spin valence bands.[56,57] The computed E_{HM} gap energies of both K_2CuVCl_6 and Rb_2CuVCl_6 materials are listed in Table 5. The E_{HM} energies obtained using the TB-mBJ–GGA approximation are increasingly higher. Therefore, the TB-mBJ–GGA results confirm the high Curie temperatures of the studied double perovskite materials, making them suitable for application in spintronic and optoelectronic devices.

3.3.2. Electronic density of states. It is essential to investigate the electron density of states (DOS) projections for each studied material in order to know the electronic details of their electronic structures. The partial density of state (PDOS) calculations were performed by employing both GGA and TB-mBJ–GGA approximations; the PDOS curves of the equilibrium K_2CuVCl_6 and Rb_2CuVCl_6 compounds are shown in Fig. 6 and 7, respectively.

For the K_2CuVCl_6 material (Fig. 6), the PDOS curves determined by the TB-mBJ–GGA scheme reveal the following: the 4s-Cu electrons in the spin-up and spin-down states appear in the energy spectra from −6 to −5 eV and from 4.5 to 8 eV, respectively; energy bands of the 4p-Cu spin-up and spin-down electrons are spotted in the energy range from −4.50 to −4 eV; the spin-up 3d-V electrons are located in the energy zones between −4.50 and −2 eV, around the Fermi level (E_F), and between 2.75 and 3.80 eV, while the spin-down 3d-V electrons are spotted in the energy regions between −4.50 and −2 eV and between 2.80 and 3.75 eV; moreover, the energy bands of the 3s-Cl spin-down electrons are located in the energy spectrum between −3.40 and −3 eV. Therefore, the PDOS of the K_2CuVCl_6 compound is mainly contributed by the 3d electrons of V atoms, where they are at the origin of the half-metallic aspect of the material. In addition, strong hybridization is also observed between the 3d-V states and the 4p-Cu states in the energy spectrum between −4.50 and −4 eV.

For the Rb_2CuVCl_6 material, Fig. 7 depicts that the bands in the energy ranges from −5.90 to −5 eV and 4.50 to 7 eV belong to the spin-up and spin-down 4s-Cu states, respectively; the energy bands between −4.50 and −3.75 eV and between 7 and 11 eV arise from the 4p-Cu spin-up and spin-down components; the spin-up and spin-down energy bands observed at around −10 eV and from 7 to 11 eV belong to the 3p states of the Cl atoms; on the other hand, the 3d-V states occupy the spin-up

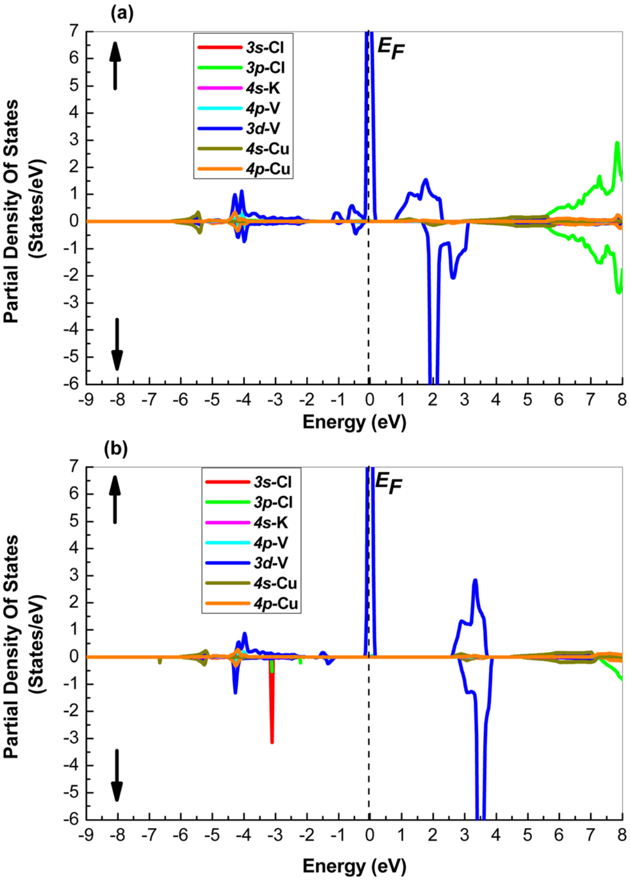

Fig. 6 Spin-polarized partial density of states (PDOS) of the equilibrium double perovskite K_2CuVCl_6 calculated using (a) PBE–GGA and (b) TB-mBJ–GGA approximations.

Table 5 Computed spin-down band gap energy E_g (in eV), half-metallic gap energy E_{HM} (in eV), and 3d-V exchange-splitting $\Delta(d)$ (in eV) of the equilibrium X_6CuVCl_6 (X = K and Rb) double perovskite materials; the results obtained using the TB-mBJ–GGA scheme are shown in parentheses

Material	E_g	E_{HM}	$\Delta(d)$
K_2CuVCl_6	1.7143 (3.8368)	0.0997 (1.1188)	2.0228 (3.4822)
Rb_2CuVCl_6	1.6055 (3.7552)	0.0333 (1.0880)	1.9438 (3.3804)
$K_2ScCuCl_6$ (ref. 44)	— (1.55)	—	—
$Rb_2ScCuCl_6$ (ref. 44)	— (1.43)	—	—

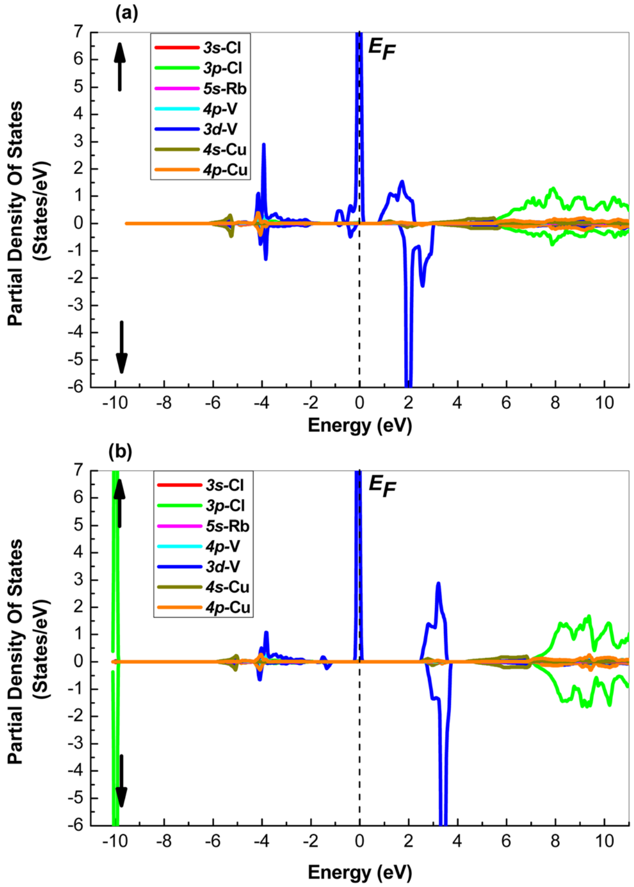

Fig. 7 Spin-polarized partial density of states (PDOS) of the equilibrium double perovskite Rb_2CuVCl_6 calculated using (a) PBE–GGA and (b) TB-mBJ–GGA approximations.

energy bands located in the energy regions from −4.25 to −2 eV, around the Fermi level (E_F), and from 2.30 to 3.50 eV; whereas, the spin-down 3d-V states lead to bands in the energy regions from −4.25 to −2 eV and 2.40 to 3.55 eV. We can conclude that the 3d-V states are responsible for the half-metallicity of the equilibrium Rb_2CuVCl_6 double perovskite as they produce an energy gap in the spin-down direction and metallic behavior in the spin-up direction around the Fermi level. Furthermore, the hybridization of the 3d-V states and the 4p-Cu states is observed in the energy range of −4.50 to −3.75 eV.

In the X_2CuVCl_6 (X = K and Rb) halide double perovskites, the 3d-V states influence the electronic structure by introducing an exchange and splitting process ($\Delta(d)$), where $\Delta(d)$ energy is defined as the energy difference between the highest d-orbital peaks of the corresponding spin-down and spin-up states.[58] It is expressed as follows:

$$\Delta(d) = E_d(\downarrow) - E_d(\uparrow) \tag{6}$$

The computed $\Delta(d)$ energy values of the studied K_2CuVCl_6 and Rb_2CuVCl_6 compounds are reported in Table 5. The TB-mBJ–GGA results are considered relatively improved owing to the high $\Delta(d)$ energy observed for the studied compounds (Table 5).

3.4. Magnetic properties

3.4.1. Computed magnetic moments. The total, interstitial and atomic moments of the equilibrium X_2CuVCl_6 (X = K and Rb) halide double perovskites were calculated by applying the FP-L/APW + lo method, and the results obtained using GGA and TB-mBJ–GGA approximations are reported in Table 6. Notably, the calculated total magnetic moments (M_{Tot}) of both materials are mainly contributed by the atomic magnetic moment of V atoms, whereas feeble contributions arise from the interstitial zone. The M_{Tot} value was found to be an integer value of 2 μ_B for both K_2CuVCl_6 and Rb_2CuVCl_6, confirming the half-metallic property of these materials. The atomic magnetic moment of the V atom is decreased compared to its free space charge of 3 μ_B, and small magnetic moments are brought into the nonmagnetic X, Cu, and Cl sites; this phenomenon is mostly due to strong p–d hybridization between the 3d-V and 4p-Cu states during the exchange and splitting process. Notably, an opposition of signs between the magnetic moments of V and Cu atoms can be seen; this means that the valence electrons of V and Cu atoms interact in an antiferromagnetic manner. Moreover, the results obtained using the framework of TB-mBJ–GGA approximation are increasingly improved.

3.4.2. Computed curie temperature. The Curie temperature (T_C) is defined in magnetic materials as the point of separation between paramagnetic and ferromagnetic configurations. We evaluated the T_C temperature according to the following equation based on the Heisenberg model:[59]

$$K_B T_C = \frac{2}{3}\sum_{i \neq j} J_{ij} \tag{7}$$

Table 6 Magnetic moments M (in μ_B) and Curie temperature T_C (in K) of the equilibrium X_6CuVCl_6 (X = K and Rb) halide double perovskites computed using the PBE–GGA and TB-mBJ–GGA functionals; the TB-mBJ–GGA-estimated values of magnetic moments are shown in parentheses

	Magnetic moment (μ_B)						Curie temperature (K)
Material	M_{Tot}	M (interstitial)	M (X)	M (Cu)	M (V)	M (Cl)	T_C
K_2CuVCl_6	2.1082 (2.0000)	0.2402 (0.2454)	0.0006 (0.0002)	−0.0133 (−0.4792)	1.9546 (2.3109)	−0.0124 (−0.0129)	814.0870
Rb_2CuVCl_6	1.9748 (2.0004)	0.2353 (0.2321)	0.0007 (0.0002)	−0.1337 (−0.4792)	1.9543 (2.3223)	−0.0137 (−0.0125)	898.1217

where J_{ij} is the exchange interaction parameter estimated according to the following formula:

$$J_{ij} = \frac{|E_{\mathrm{FM}} - E_{\mathrm{AFM}}|}{2} \quad (8)$$

The calculated T_C temperatures of the equilibrium X_2CuVCl_6 (X = K and Rb) halide double perovskites using the TB-mBJ–GGA scheme are listed in Table 6. Notably, the T_C values of both compounds are high.

4. Conclusions

In summary, the FP-LAPW + lo method was applied in this work to evaluate the structural, elastic, electronic and magnetic properties of X_2CuVCl_6 (X = K and Rb) halide double perovskite compounds at equilibrium. The main conclusions of this prediction model are summarized below:

(i) Analyses of the structural properties of both compounds show that the ferromagnetic state is the stable ground phase.

(ii) The optimized structural parameters (a_0, B_0, B' and E_0) of the compounds are reported in this study.

(iii) The calculated elastic constants of both materials confirm their mechanical stability and ductility.

(iv) The calculated electronic properties of the compounds using both GGA and TB-mBJ–GGA parameterizations prove that they are entirely half-metals with a large half-metallic gap.

(v) The half-metallic gaps corresponding to the two halide double perovskites are calculated using GGA and TB-mBJ–GGA functionals.

(vi) The 3d-V exchange-splitting energy ($\Delta(d)$) calculated using this approach was found to be large for both studied compounds.

(vii) The estimated magnetic properties of the two compounds reveal that:

(1) The atomic magnetic moment of the V atom contributes mainly to the total magnetic moment.

(2) The opposite signs of the atomic magnetic moments of V and Cu atoms reveal that the valence electrons of V and Cu atoms interact in an antiparallel manner during the exchange and splitting process.

(3) The hybridization between 3d-V and 4p-Cu electrons reduces the magnetic moment of the V atom from its free space charge and produces weak magnetic moments at the non-magnetic X, Cu and Cl sites.

Data availability

Data supporting the results presented in this paper are not publicly available at this time but may be obtained from the corresponding author (fatmimessaud@yahoo.fr) upon reasonable request.

Conflicts of interest

The authors declare that they have no conflict of interest.

Acknowledgements

The authors extend their appreciation to the Deanship of Scientific Research at Northern Border University, Arar, KSA for funding this research work through the project number NBU-FFR-2025-310-11.

References

1 W. E. Pickett and J. S. Moodera, *Phys. Today*, 2001, **54**, 39–44.
2 R. A. de Groot, F. M. Mueller, P. G. van Engen and K. H. J. Buschow, *Phys. Rev. Lett.*, 1983, **50**, 2024–2027.
3 R. J. Soulen Jr, J. M. Byers, M. S. Osofsky, B. Nadgorny, T. Ambrose and A. Barry, *Science*, 1998, **282**, 85–88.
4 K. L. Kobayashi, T. Kimura, H. Sawada, K. Terakura and Y. Tokura, *Nature*, 1998, **395**, 677–680.
5 I. Galanakis, *Phys. Rev. B:Condens. Matter Mater. Phys.*, 2005, **71**, 012413.
6 S. Wurmehl, G. H. Fecher, H. C. Kandpal, V. Ksenofontov, C. Felser and H.-J. Lin, *Appl. Phys. Lett.*, 2006, **88**, 032503.
7 M. Nakao, *Phys. Rev. B:Condens. Matter Mater. Phys.*, 2004, **69**, 214429.
8 A. Nfissi, R. El Fdil, A. Samih, D. Kabouchi, Z. Fadil, C. J. Raorane, A. A. Ifseisi, M. E. Assal and E. Salmani, *J. Magn. Magn. Mater.*, 2024, **610**, 172563.
9 A. Nfissi, D. Kabouchi, R. El Fdil, A. Samih, Z. Fadil, C. J. Raorane, K. H. Mahmoud, A. S. A. Alsubaie and E. Salmani, *Solid State Commun.*, 2024, **389**, 115596.
10 G. Li, Z. Li and Z. Liu, *J. Magn. Magn. Mater.*, 2025, **614**, 172742.
11 B. Gurunani and D. C. Gupta, *Mater. Sci. Eng., B*, 2025, **311**, 117783.
12 F. Firdous, Q. Ain, S. A. M. Issa, H. M. H. Zakaly and J. Munir, *RSC Adv.*, 2024, **14**, 34679–34689.
13 I. Muhammad, S. Ahmed, N. Ullah, M. Mushtaq, M. Liaqat, X. Tian and J.-M. Zhang, *Results Phys.*, 2024, **57**, 107419.
14 F. Faid, H. Mebarki, K. Mokadem, F. M. Abdalilah, A. Benmakhlouf, M. Khatiri and T. Helaimia, *J. Magn. Magn. Mater.*, 2024, **605**, 172345.
15 J. K. Sharma, A. Dhamija, A. Pal and J. Kumar, *Comput. Mater. Sci.*, 2024, **232**, 112679.
16 M. Jamil, M. Manzoor, A. Kumar, A. Agrawal, R. Almeer, Y. A. Kumar and R. Sharma, *Solid State Commun.*, 2024, **394**, 115702.
17 H. Kerrai, A. Zaim and M. Kerouad, *Vacuum*, 2024, **226**, 113341.
18 M. Y. Sofi, M. S. Khan and M. A. Khan, *Mater. Sci. Semicond. Process.*, 2025, **186**, 109023.
19 M. A. Yasir, G. M. Mustafa, M. A. Ameer, N. A. Noor, S. Mumtaz and I. M. Moussa, *Mater. Sci. Eng., B*, 2025, **311**, 117830.
20 M. Husain, H. Albalawi, M. Al Huwayz, N. Al Saqri, R. Khan and N. Rahman, *Phys. Scr.*, 2023, **98**, 105935.
21 N. Rahman, A. Rauf, M. Husain, N. Sfina, V. Tirth, M. Sohail, R. Khan, A. Azzouz-Rached, G. Murtaza, A. A. Khan and S. A. Khattak, *RSC Adv.*, 2023, **13**, 15457–15466.

22 M. Husain, N. Rahman, H. Albalawi, S. Ezzine, M. Amami, T. Zaman, A. U. Rehman, M. Sohail, R. Khan, A. A. Khan, Tahir and A. Khan, *RSC Adv.*, 2022, **12**, 32338–32344.

23 S. A. Shah, M. Husain, N. Rahman, M. Sohail, R. Khan, A. Alataway, A. Z. Dewidar, H. O. Elansary, L. Abu El Maati, K. Yessoufou, A. Ullah and A. Khan, *Materials*, 2022, **15**, 5684.

24 S. A. Shah, M. Husain, N. Rahman, M. Sohail, R. Khan, A. A. Khan, A. Ullah, S. A. M. Abdelmohsen, A. M. M. Abdelbacki, A. M. El-Sabrout, H. O. Elansary and A. Khan, *RSC Adv.*, 2022, **12**, 8172–8177.

25 N. Rahman, M. Husain, V. Tirth, A. Algahtani, H. Alqahtani, T. Al-Mughanam, A. H. Alghtani, R. Khan, M. Sohail, A. A. Khan, A. Azzouz-Rached and A. Khan, *RSC Adv.*, 2023, **13**, 18934–18945.

26 A. A. Pasha, H. Khan, M. Sohail, N. Rahman, R. Khan, O. H. Alsalmi, D. Abduvalieva, K. M. Abualnaja, A. El Jery and M. Adrdery, *Mater. Adv.*, 2023, **4**, 6645–6654.

27 W. Ullah, M. Husain, N. Rahman, N. Sfina, M. Elhadi, R. Khan, M. Sohail, A. Azzouz-Rached, M. Uzair, A. A. Khan and A. Khan, *Silicon*, 2024, **16**, 3021–3032.

28 U. Hameed, H. Ullah, S. Z. Abbas, K. Safeen, K. M. Alotaibi, A. Safeen, S. Yasin, G. Murtaza, F. Khalil, S. Ali, G. Asghar and R. Khan, *J. Phys. Chem. Solids*, 2025, **199**, 112519.

29 M. S. Khan, M. Sohail, N. Rahman, R. Khan, H. E. Ali, J. Jamil, B. S. Abdullaeva, K. M. Abualnaja, G. Alosaimi, Y. Khairy and H. Algarni, *Chem. Pap.*, 2025, **79**, 107.

30 N. S. Alsaiari, I. Ahmed, S. Hanf, M. M. Rekha, M. Kundlas, M. Ouladsmane, K. Muhammad and J. Rehman, *J. Inorg. Organomet. Polym.*, 2025, DOI: 10.1007/s10904-025-03746-z.

31 N. Rahman, K. M. Abualnaja, S. Belhachi, N. Sfina, M. Husain, B. M. Al-Khamiseh, A. Azzouz-Rached, H. A. Althobaiti, S. Ullah, R. Khan and M. Asghar, *J. Inorg. Organomet. Polym.*, 2025, **35**, 1439–1452.

32 N. Sfina, N. Rahman, S. Belhachi, M. Husain, B. M. Al-Khamiseh, K. M. Abualnaja, G. Alosaimi, A. Azzouz-Rached, S. Ullah, A. U. Rashid and R. Khan, *J. Inorg. Organomet. Polym.*, 2024, **34**, 6102–6113.

33 M. Husain, N. Rahman, A. Azzouz-Rached, N. Sfina, K. M. Abualnaja, G. Alosaimi, M. Asad, R.-D. Hamza, V. Tirth, N. U. Khan, Q. Humayun, R. Khan, R. Ahmad, A. Samreen, A. A. Khan and J. Lu, *Inorg. Chem. Commun.*, 2024, **164**, 112424.

34 P. Hohenberg and W. Kohn, *Phys. Rev.*, 1964, **136**, B864.

35 K. M. Wong, S. M. Alay-e-Abbas, A. Shaukat, Y. Fang and Y. Lei, *J. Appl. Phys.*, 2013, **113**, 014304.

36 K. M. Wong, S. M. Alay-e-Abbas, Y. Fang, A. Shaukat and Y. Lei, *J. Appl. Phys.*, 2013, **114**, 034901.

37 P. Blaha, K. Schwarz, P. Sorantin and S. K. Trickey, *Comput. Phys. Commun.*, 1990, **59**, 339.

38 J. P. Perdew, S. Burke and M. Ernzerhof, *Phys. Rev. Lett.*, 1996, **77**, 3865–3868.

39 F. Tran and P. Blaha, *Phys. Rev. Lett.*, 2009, **102**, 226401.

40 D. Koller, F. Tran and P. Blaha, *Phys. Rev. B:Condens. Matter Mater. Phys.*, 2011, **83**, 195134.

41 G. M. Mustafa, R. Waqar, S. Saba, N. A. Noor, Z. Farooq, M. Imran, R. B. Behram and Y. M. Alanazi, *Phys. Scr.*, 2023, **98**, 065703.

42 F. D. Murnaghan, *Proc. Natl. Acad. Sci. U. S. A.*, 1944, **30**, 244–247.

43 S. L. Shang, Y. Wang, D. Kim and Z.-K. Liu, *Comput. Mater. Sci.*, 2010, **47**, 1040–1048.

44 A. Ayyaz, G. Murtaza, A. Usman, N. Sfina, A. S. Alshomrany, S. Younus, S. Saleem and Urwa-tul-Aysha, *J. Inorg. Organomet. Polym.*, 2024, **34**, 3560–3575.

45 J. J. Kim, H. W. Seong and H. J. Ryu, *J. Nucl. Mater.*, 2022, **566**, 153780.

46 A. Yakoubi, O. Baraka and B. Bouhafs, *Results Phys.*, 2012, **2**, 58–65.

47 J. B. Kramers-Kronig, *Am. J. Phys.*, 2011, **79**, 1053–1059.

48 M. Born and K. Huang, *Dynamical Theory of Crystal Lattices*, Clarendon, Oxford, 1956.

49 J. Wang and S. Yip, *Phys. Rev. Lett.*, 1993, **71**, 4182.

50 W. Voigt, *Lehrbuch der Kristallphysik*, Taubner, Leipzig, 1928.

51 A. Reuss, *Z. Angew. Math. Mech.*, 1929, **9**, 55.

52 R. Hill, *Proc. Phys. Soc., London*, 1953, **65**, 909.

53 G. Vaitheeswaran, V. Kanchana, R. S. Kumar, A. L. Cornelius, M. F. Nicol, A. Svane, A. Delin and B. Johansson, *Phys. Rev. B:Condens. Matter Mater. Phys.*, 2007, **76**, 014107.

54 S. F. Pugh, *Philos. Mag.*, 1954, **45**, 823.

55 G. Simmon and H. Wang, *Single Crystal Elastic Constants and Calculated Aggregate Properties: a Handbook*, M.I.T Press, Cambridge, 1971.

56 K. L. Yao, G. Y. Gao, Z. L. Liu and L. Zhu, *Solid State Commun.*, 2005, **133**, 301–304.

57 G. Y. Gao, K. L. Yao, E. Sasioglu, L. M. Sandratskii, Z. L. Liu and J. L. Jiang, *Phys. Rev. B:Condens. Matter Mater. Phys.*, 2007, **75**, 174442.

58 A. Zunger, *Solid State Phys.: Condens. Matter*, 1986, **39**, 275.

59 J. Kubler, G. H. Fecher and C. Felser, *Phys. Rev. B:Condens. Matter Mater. Phys.*, 2007, **76**, 024414.